

Cellular Organization and Substructure Measured Using Angle-Resolved Low-Coherence Interferometry

Adam Wax,* Changhuei Yang,* Vadim Backman,* Kamran Badizadegan,† Charles W. Boone,*
Ramachandra R. Dasari,* and Michael S. Feld*

*G. R. Harrison Spectroscopy Laboratory, Massachusetts Institute of Technology, Cambridge Massachusetts 02139 and

†Department of Pathology, Children's Hospital and Harvard Medical School, Boston, Massachusetts 02115 USA

ABSTRACT We measure the organization and substructure of HT29 epithelial cells in a monolayer using angle-resolved low-coherence interferometry. This new technique probes cellular structure by measuring scattered light, as in flow cytometry, but offers an advantage in that the structure can be examined in situ, avoiding the need to disrupt the cell monolayer. We determine the size distribution of the cell nuclei by fitting measured light-scattering spectra to the predictions of Mie theory. In addition, we obtain information about the cellular organization and substructure by examining the spatial correlations within the monolayer. A remarkable finding is that the spatial correlations over small length scales take the form of an inverse power law, indicating the fractal nature of the packing of the subcellular structures. We also identify spatial correlations on a scale large compared with the size of a cell, indicating an overlying order within the monolayer.

INTRODUCTION

Examining the structural features of cells is essential for many clinical and laboratory studies. The most common tool for studying cellular features is histology, by which cells are examined using a microscope after they are fixed, stained, and thinly sliced. Although this approach has led to many great advances in understanding cell structure and function, it is inherently limited by the artifacts of preparation. Specifically, the characteristics of the cells are only seen at one moment in time and their structural features are altered because of the addition of chemicals. In histopathology, where the clinical goal is to diagnose disease, these artifacts are acceptable; however, in cell biology studies, in which one is trying to obtain an understanding of the structure and function of the cell, it is greatly advantageous to examine living cells.

The structure of intact, living biological cells can be investigated by examining their angular scattering characteristics. Angle-resolved light-scattering distributions are conventionally obtained using a goniometer (Drezek et al., 1999). However, this technique has limitations. In goniometry, carefully prepared suspensions of cells are needed to avoid the effects of multiple scattering. Structural information can also be obtained via light-scattering in flow cytometry (Givan, 2001). However, with this approach, cells samples must be disrupted as they are flowed through the apparatus to analyze them. Recently, we have developed angle-resolved low-coherence interferometry (a/LCI), a

means for measuring the angular distribution of back-scattered light based on a modified Michelson interferometer (Wax et al., 2001c). This approach can noninvasively probe the structure of an arbitrary cell sample. Because a/LCI is implemented using a low-coherence source, it enables light scattered from a localized region to be selectively detected, even for subsurface layers (to a depth of 1 mm). This method has been applied to determine the size distribution of polystyrene microsphere suspensions with subwavelength precision (Wax et al., 2001a). In this paper we establish the utility of a/LCI for probing structural and organizational features of intact, living cells.

Recent interest in the clinical use of light-scattering techniques to measure cell properties has focused on determining the size of cell nuclei to aid diagnosis of disease. In particular, light-scattering spectroscopy (LSS) has shown that cell nuclei can be modeled as spherical Mie objects and their size distribution determined by comparing the wavelength dependence of their back-scattering cross-section with theoretical models (Perelman et al., 1998). This technique has been demonstrated as an effective means of detecting abnormalities in epithelial cell nuclei associated with neoplasia, a precancerous state (Backman et al., 2000). A more recent implementation of LSS measures the spectrum of scattered light at various scattering angles to obtain information about both the cell nuclei and smaller structures (Backman et al., 2001).

The a/LCI technique is an interferometry-based implementation of LSS. In conventional LSS techniques, scattered intensity is measured and polarization-gating or modeling is used to isolate singly scattered light by rejecting the contributions of multiply scattered photons. a/LCI is an alternative method for isolating single scattering and, unlike LSS, it provides optical sectioning, the ability to selectively probe subsurface layers to construct depth-resolved tomographic images. Early efforts to implement LSS using interferometry sought to include multiple wavelengths of

Submitted October 17, 2001, and accepted for publication January 15, 2002.

Address reprint requests to Adam Wax, 77 Massachusetts Avenue, MIT Spectroscopy Laboratory, Room 6–014, Cambridge Massachusetts 02139. Tel.: 617-258-9404; Fax: 617-253-4513; E-mail: awax@mit.edu.

V. Backman's current address: Department of Biomedical Engineering, Northwestern University, Evanston, IL 60208.

© 2002 by the Biophysical Society

0006-3495/02/04/2256/09 \$2.00

broadband light in a Michelson interferometer (Yang et al., 2000). Here, we take a different approach and recover structural information by examining the angular distribution of back-scattered light using a single broadband light source. We measure the transverse component of the momentum transfer associated with the light-scattering process by mixing the light back-scattered by a sample with a reference field with a variable transverse momentum, i.e., angle of propagation. This technique is closely related to a previous interferometric method for measuring the optical phase-space distribution of a light field (Wax and Thomas, 1996).

The purpose of this paper is to demonstrate that the structural features of living cells in an intact monolayer can be measured quantitatively and noninvasively using the a/LCI technique. We measure the angular distributions of light back-scattered by monolayers of intestinal epithelial cells. We demonstrate that the size distribution of the cell nuclei can be determined with subwavelength precision by comparing the oscillatory part of measured angular distributions to the predictions of Mie theory. In addition, we analyze correlations in the light-scattering data to obtain information about the organization of the subcellular structures, as well as that of the cell monolayer as a whole.

EXPERIMENTAL SETUP

Low-coherence interferometry

The a/LCI scheme uses a modified Michelson interferometer (Fig. 1). Broadband light from a superluminescent diode (superluminescent diode (SLD) (EG&G, Gaithersburg, MD), output power 3 mW, center wavelength 845 nm, full width half-maximal bandwidth 22 nm) with a coherence length of $l_c = 2 \ln 2/\pi \times \lambda^2/\Delta\lambda = 14.3 \mu\text{m}$ is divided by a beamsplitter (BS) into a reference beam and an input beam to the sample. The reference beam is reflected by a mirror (M) and recombined at BS with light reflected by the sample. The mixed fields generate an interference pattern provided that the two optical path-lengths are matched to within the coherence length of the source. To separate the interference signal from the total intensity and low-frequency noise, a heterodyne signal is generated by translating the reference M at a constant velocity (4 mm/s). This causes the heterodyne beat intensity to oscillate at the corresponding Doppler-shifted frequency (9.5 kHz). The beat intensity is determined by calculating the power spectrum of the digitized photocurrent (sampled at 333 kHz) and bandpassing the signal at the heterodyne frequency. This yields a signal that is linearly proportional to the squared amplitude of the detected signal field. (It has been previously noted in Wax and Thomas (1996) that by measuring the mean square heterodyne beat, the detected signal is related to the Wigner distribution of the signal field convoluted

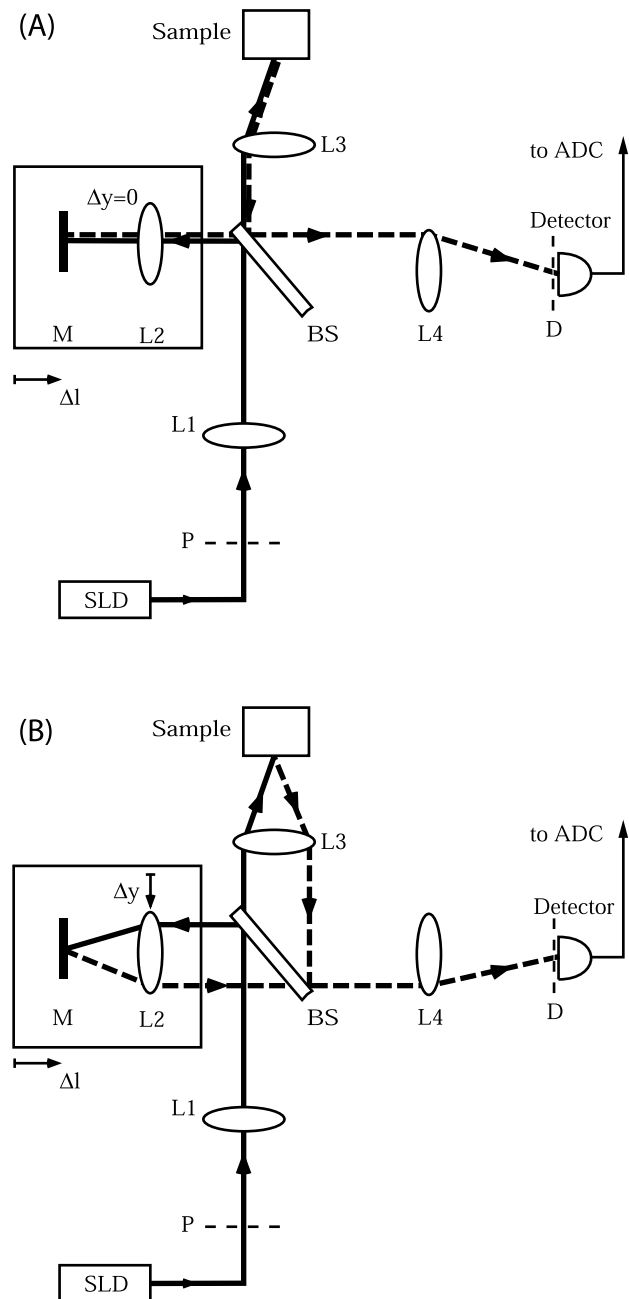


FIGURE 1 (A) Schematic of the interferometer system illustrating the detection of back-scattered light. The photocurrent is digitized by an analog-to-digital converter (ADC) and recorded using a PC. The distances between elements are: plane P to $L1 = 10 \text{ cm} = f_1$, $L1$ to $BS = 10 \text{ cm}$, BS to $L2 = 4.5 \text{ cm} = f_2$, $L2$ to $M = 4.5 \text{ cm}$, BS to $L3 = 4.5 \text{ cm} = f_3$, $L3$ to sample = 4.5 cm , BS to $L4 = 10 \text{ cm} = f_4$, $L4$ to plane $D = 10 \text{ cm}$. (B) Schematic of the interferometer system illustrating the displacement of lens $L2$ to vary the angle that the reference beam crosses the detector plane.

with that of the reference field. In the current experiments, the angular resolution is sufficiently small that we can regard our signal as the Wigner distribution of the back-scattered field.)

a/LCI

The a/LCI spectra depict the mean square heterodyne signal as a function of scattering angle, referenced to the exact back-scattering direction. The a/LCI system uses four achromatic imaging lenses (L1-L4, focal lengths f_1 - f_4) to permit the measurement of angular scattering distributions. These lenses are arranged to form multiple $4f$ imaging systems, which image both the phase and amplitude of the light field (Wax et al., 2001a, 2001b). The reference field is made to cross-the detector plane at a variable angle by scanning lens L2 ($f_2 = 4.5$ cm) a distance Δy perpendicular to the beam path. It can be shown using Fourier optics that this translation causes the reference field to be reproduced in the plane of the detector (D) with its angle of propagation changed by $\theta_T = 2 \Delta y/f_2$ but its position unchanged (Wax et al., 2001b). Fig. 1, *A* and *B* illustrate the effects of transversely scanning L2 in the imaging system using ray traces. It can be seen that light is collected at a specific angle relative to the exact back-scattering direction.

Because LCI relies on matching the path-length of light in both the reference and signal arms to obtain depth resolution, L2 is moved in conjunction with the reference mirror M longitudinally along the direction of the beam path while the length of the reference arm is varied. This ensures that the path-length of the light through the system remains unchanged as L2 is translated.

Another important feature of the a/LCI system is the lateral displacement of lens L3 relative to lens L1. This translation results in the input beam entering the sample at an angle of 240 mrad (13.8°) and permits the full angular aperture of the lens to be used to collect angular back-scattering data, rather than only the half-angle that would be possible with normal incidence. In the current scheme, the maximum clear aperture limits the angular scans to a total range of 480 mrad (27.5°). The angular resolution, $\theta_{\text{res}} = 1.4$ mrad (0.08°), is given by the diffraction angle of the 0.45-mm diameter collimated beam incident on the sample. Because the angular distributions we seek to measure are symmetric about the exact back-scattering direction, the system is implemented so that the scan begins in the exact back-scattering direction and extends 480 mrad away from that direction. As discussed above, the light enters the sample at an angle of 240 mrad relative to the sample surface. Note, however, that the exact back-scattering direction is antiparallel to the input beam, regardless of the orientation of the sample surface.

Cell cultures

Differentiated intestinal epithelial cells HT29 (gift of the Harvard Digestive Diseases Center) were grown in LabTek chambered coverglasses (Nalge Nunc International, Naperville, IL) using high-glucose Dulbecco modified Eagle medium supplemented with 10% fetal calf serum, 100 units/ml

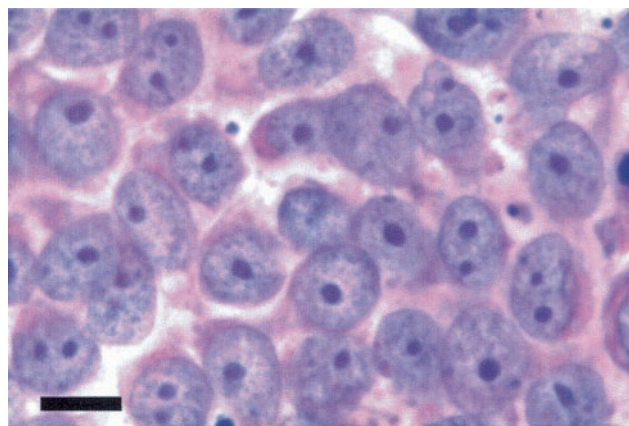


FIGURE 2 Photomicrograph of a typical HT29 cell monolayer after fixation and staining. Length scale indicated by the 10- μm bar. Note that the outlines of individual cells are difficult to see in this micrograph and should not be confused with those of the cell nuclei which are more clearly delineated. Similarly, the nucleolus should not be confused for the nucleus itself.

penicillin and 100 $\mu\text{g/ml}$ streptomycin (all from Gibco BRL, Life Technologies, Grand Island, NY). Cells were grown to confluency at 37°C in a humidified atmosphere of 5% CO_2 in air. For the experiments, monolayers were transferred to Hank Balanced Salt Solution without sodium bicarbonate or phenol red, buffered at pH 7.4 with 10 mM HEPES (all chemicals from Sigma, St. Louis, MO). Fig. 2 shows a photomicrograph of a typical monolayer of HT29 cells which have been fixed in formalin and stained with hemotoxalin and eosin. The nuclei and some subnuclear structure of these cells, such as the nucleoli and the heterochromatin clumps, are visible.

DATA ANALYSIS

The a/LCI spectra for the epithelial cells consist of a number of components. Structural information about the cells is obtained by analyzing these components using various theoretical models. The light scattered by the cell nucleus is compared with the predictions of Mie theory, an analytical treatment of light scattering by dielectric spheres. The light scattered by smaller structures within the cell is analyzed by identifying the spatial correlation of the structures. The spatial correlations are also analyzed to yield information about long-range correlations within the monolayer. This section describes how the various components are separated and how each component is used to determine structural information about the cells.

Mie scattering by cell nuclei

Mie theory provides an exact analytical solution for the angular spectrum of light at wavelength λ scattered by a sphere of diameter d and relative refractive index n . The

parallel and perpendicular polarization components of the scattered light field can be obtained by calculating the scattering amplitudes $S_2(\theta, \phi)$ and $S_1(\theta, \phi)$, respectively (van de Hulst, 1957). In the current experiments, broadband light containing many wavelength components is scattered by an ensemble of spheroidal cell nuclei with a polydisperse size distribution. To include the effects of broad distributions in both wavelength and size, an overall distribution in size parameter, $x = \pi d/\lambda$, is calculated. If it is assumed that both the wavelengths and sizes are Gaussian distributed, then the effect is a Gaussian distribution of size parameters with a width given by

$$\left(\frac{\Delta x}{x}\right)^2 = \left(\frac{\Delta \lambda}{\lambda}\right)^2 + \left(\frac{\Delta d}{d}\right)^2,$$

where Δx is the $1/e$ width of the resulting Gaussian distribution. The component of the scattered field for each size parameter is calculated using Mie theory, and the Gaussian distribution of size parameters is used as a weighting function in summing these contributions to the total scattered field.

Previous LSS studies have shown that light scattered by cell nuclei can be modeled using Mie theory (Perelman et al., 1998). In these studies, the oscillatory part of the light-scattering spectrum in inverse wavelength space is compared with Mie theory to make a size determination. The current experiments make a size determination by examining the oscillatory component of the angular variations in the a/LCI spectrum at a fixed wavelength. The two methods are complimentary in that both measure the momentum transfer associated with the elastic scattering process.

The measured a/LCI spectra are initially fit to a fourth-order polynomial, which is then subtracted from the data to yield its oscillatory component in θ . This is an essential step in separating the light-scattering contribution of the nucleus from that of other subcellular structures, as both components have slowly varying backgrounds. However, the light-scattering patterns exhibit oscillations that rise in frequency with particle size. Because the nucleus is the largest of the subcellular organelles, only the contribution from the nucleus exhibits characteristic high-frequency oscillations.

To make an accurate size determination through comparison to Mie theory, the data are further processed by suppressing high-frequency oscillations arising from long-range, intercellular correlations. These oscillations contain important information about the organization of the cell monolayer, but can interfere with determining the size of cell nuclei. Thus, oscillations in the a/LCI spectra attributable to correlations which are larger than the size of the cell ($>16 \mu\text{m}$) are suppressed during this portion of the analysis by applying a step-function filter to the data in Fourier space.

The extracted oscillatory component of the light-scattering data is compared with the predictions of Mie theory to

determine the structure of the cell nuclei. For this purpose, a numerical database of scattering distributions was created which contains calculated angular scattering patterns for a range of diameters ($5.0\text{--}15.0 \mu\text{m}$, in $0.1\text{-}\mu\text{m}$ increments), a range of size distributions (the $1/e$ width of the Gaussian distributions are 1, 2.5, 5, 7.5, and 10% of the mean diameter) and a range of relative refractive indices (36 discrete values between 1.01 and 1.08). These values were selected from the literature to encompass the properties of healthy cells (Tuchin, 2000) and those of immortal cell lines (Backman et al., 1999).

To compare the theoretical distributions with the experimental data, each calculated distribution is fit to a fourth-order polynomial, which is then subtracted from the theoretical distribution to leave only the oscillatory component. A fourth-order polynomial was selected as it contains the major features of the slowly varying background over the angular range of the data. The remaining oscillatory part of the experimental data is compared with the oscillatory part of the various theoretical distributions by computing the χ^2 value for each. The structure of the cell nuclei, i.e., their size, size distribution, and relative refractive index, is then determined by minimizing this χ^2 value.

Fractal organization of smaller cell structures

Once the contribution from the nucleus has been identified using the above analysis, it is subtracted from the filtered a/LCI spectrum to yield the component of the light scattering arising from the smaller structures. This component is analyzed to determine the organization of the smaller structures.

The angular distribution of scattered intensity, i.e., the squared magnitude of the field $|E(\vec{\theta})|^2$, is related to the two-point spatial correlation function of the optical field, $\Gamma_E(r)$, through a Fourier transform (Mandel and Wolf, 1995):

$$\begin{aligned} \Im[|E(\vec{\theta})|^2] &= \int e^{ik\vec{\theta}\vec{r}} |E(\vec{\theta})|^2 d^2(k\vec{\theta}) \\ &= \langle E(\vec{r}') E^*(\vec{r}' + r\hat{\theta}) \rangle \equiv \Gamma_E(r) \end{aligned} \quad (1)$$

In this expression, k is the magnitude of the optical wave-vector, and r is the length scale of the spatial correlations along the transverse direction given by the angle θ .

In the case where the spatial variations in the electric field arise from interactions with an inhomogeneous medium, such as the internal structure of a cell, the component of the scattered electric field for each spatial frequency can be related to similar variations in the dielectric constant of the inhomogeneous medium which caused the scattering (Landau and Lifshitz, 1960):

$$E(\vec{k}_\perp) \approx \vec{k}\vec{\theta} \propto \partial \varepsilon(\vec{k}_\perp). \quad (2)$$

Here \vec{k}_\perp represents the transverse component of the optical wave-vector, whereas

$$\partial\varepsilon(\vec{k}_\perp) \equiv \int d^2\vec{r}_\perp e^{i\vec{k}_\perp \cdot \vec{r}_\perp} \partial\varepsilon(\vec{r}_\perp) \quad (3)$$

is the Fourier transform of the spatial variations in the dielectric constant of the inhomogeneous medium. In this discussion, we are concerned with the component of the wave-vector and the length scale of the spatial correlations perpendicular to the optical axis, defined by $\theta = 0$, the exact back-scattering direction.

The scattered electric field can be related to variations in density by assuming that the variations in the dielectric constant arise from corresponding fluctuations in the density of the medium, $\partial\rho(\vec{r}_\perp)$:

$$\begin{aligned} \Gamma_E(r) &= \langle E(\vec{r}_\perp') E^*(\vec{r}_\perp' + r\hat{\theta}) \rangle \\ &\propto \langle \partial\rho(\vec{r}_\perp') \partial\rho(\vec{r}_\perp' + r\hat{\theta}) \rangle \equiv \Gamma_\rho(r), \end{aligned} \quad (4)$$

where $\Gamma_\rho(r)$ is the two-point correlation function of the density fluctuations along the direction defined by the angle θ .

As described below, we find that the small structure component of the a/LCI spectra takes the form of a power law distribution in θ , where θ is the scattering angle relative to the back-scattering direction. This leads to an inverse power law in the two-point correlation function. We find that the density variations scale as:

$$\Gamma_\rho(r) \propto r^{-\alpha} \quad (5)$$

where α is the power law exponent, which is found by fitting the Fourier transformed data.

The fact that the spatial dependence of the correlation function takes the form of an inverse power law indicates the fractal or self-similar nature of the sample. The self-similarity in this case can be seen by considering a change in length scale by a factor λ , which yields (Teixera, 1986):

$$\Gamma(\lambda r) \propto (\lambda r)^{-\alpha} = \lambda^{-\alpha} r^{-\alpha} \propto \lambda^{-\alpha} \Gamma(r). \quad (6)$$

This expression indicates that the correlations within the object are scale-invariant, revealing its fractal nature.

Fractal organization of structure is usually defined in terms of a fractal dimension D . For the case of a mass fractal, the fractal dimension is defined by

$$M(r) \propto r^D, \quad (7)$$

where $M(r)$ is the mass enclosed by a sphere of radius r . In the case of an object with uniform density, the value of D is 3, the same as the Euclidean dimension. For an object with fractal organization, however, the value of D is less than the Euclidean dimension.

The fractal dimension can easily be related to the power law exponent, α . The spatial dependence of the mass func-

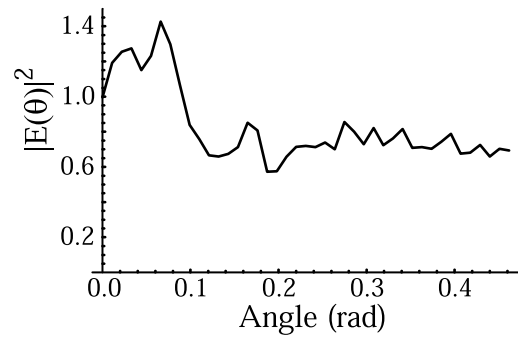


FIGURE 3 Typical a/LCI spectra from HT29 epithelial cells. The spectra are shown as the mean square heterodyne signal as a function of scattering angle, relative to the exact back-scattering direction. The data are normalized to the scattered intensity in the exact backward direction.

tion is related to that of the correlation function by (Teixera, 1986):

$$M(r') = \int_0^{r'} d^3r \frac{\Gamma(r)}{\bar{\rho}} \propto \int_0^{r'} d^3r r^{-\alpha} \propto r^{3-\alpha}, \quad (8)$$

where $\bar{\rho}$ is the average density of the object. Comparing Eq. 8 with Eq. 7, we identify the relationship between the fractal dimension and the power law exponent:

$$D = 3 - \alpha. \quad (9)$$

The concept of a fractal dimension will be used in analyzing the organization of the smaller structures within the cells.

Long-range correlations

Eqs. 1–4, which identify the relationship between the scattered electric field and the density correlations of the scattering sample, can also be used to identify long-range correlations within a histological structure. Increases in the density correlation function (Eq. 4) compared with the background density indicate correlations at corresponding length scales. In our light-scattering data, we identify correlations which extend well beyond the size of an individual cell by examining such increases in the density correlation function.

RESULTS

Fig. 3 shows a typical a/LCI spectrum for interferometrically detected light, scattered by an HT29 epithelial cell monolayer. The square of the magnitude of the scattered field is plotted as a function of the scattering angle relative to the exact back-scattering direction. The Fourier transform of these data yields the two-point correlation function of the sample, as described by Eqs. 1–4. Fig. 4 shows the two-point correlation function obtained from the data of Fig. 3. Using the analysis methods described above, the data rep-

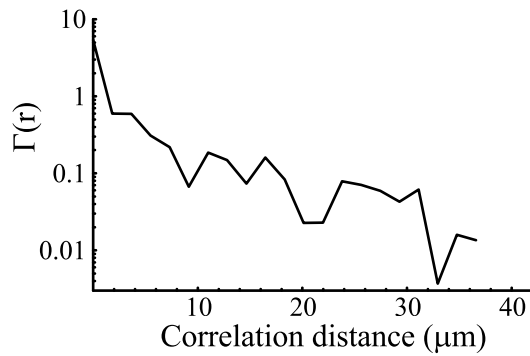


FIGURE 4 Two-point correlation function $\Gamma(r)$ of the light field scattered by HT29 epithelial cells resulting from the data of Fig. 3.

resented in these two figures yield structural and organizational information about the cell monolayer.

Size distribution of cell nuclei

The size distribution of the cell nuclei is obtained by comparing the angular scattering distribution with the predictions of Mie theory. However, the organization of the monolayer can complicate this comparison. In particular, as the cells in the monolayer are fairly regularly spaced, the coherent nature of the illuminating light results in interference of light scattered by adjacent cells. This can be seen in Fig. 4, which shows the existence of correlations that are larger than the size of the cells (typically 10–15 μm). For the purpose of determining the size of the cell nuclei, these correlations are suppressed during this part of the analysis by filtering the data, as described above.

The presence of smaller structures in the cells can also influence the determination of the size of the cell nuclei. Simply minimizing the χ^2 value between the raw data in Fig. 3 and various theoretical distributions does not always yield a correct size determination. The smaller structures within the cell and nucleus produce a slowly varying background in the a/LCI spectrum. However, the larger cell nucleus produces both a slowly varying background and high-frequency oscillations in the a/LCI spectrum. Thus, the total background of the a/LCI spectrum is altered by the presence of the smaller particles, but the high-frequency component remains unchanged. The change in the overall slope causes the χ^2 minimization algorithm to lead to incorrect sizes as the best match to the background is selected instead of matching the periodicity of the high frequency component. To overcome this, the background is removed from the light-scattering data by first fitting it to a fourth-order polynomial, leaving the high-frequency oscillatory components. The resulting oscillatory distribution, characteristic of the larger sized nuclei, is then compared with Mie theory to yield the size of the cell nuclei.

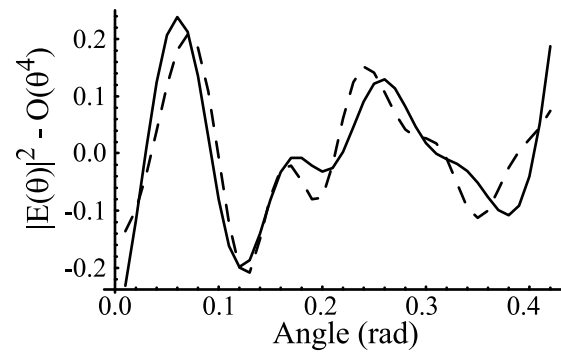


FIGURE 5 Oscillatory part of the light-scattering data (*solid line*) compared with the best fit theoretical distribution (*dashed line*) obtained using Mie theory. This part of the light-scattering data is used to extract the size and size distribution of the epithelial cell nuclei.

Fig. 5 shows the oscillatory part of the light-scattering data extracted using the methods described previously. To determine the structural properties of the cell nuclei, the oscillatory part of the distribution is compared with similarly extracted components of theoretical distributions calculated using Mie theory. The best fit is found by minimizing the χ^2 value between the processed data and theory. For the data (*solid line*) of Fig. 5, the best fit (*dashed line*) is obtained for a theoretical distribution of light scattered by a Gaussian distribution of spherical particles with a refractive index mismatch of $1.46/1.37 = 1.066$, a 9.7- μm mean diameter and a $1/e$ width of 5% (0.49 μm).

In the experiments, angular light-scattering data were obtained from four cell monolayer samples. Randomly sampled spatial points, 0.45 μm in diameter, were examined on each sample. The size distribution of the cell nuclei, as well as correlation information about the remaining cell structures and the monolayer itself, were obtained from 12 a/LCI spectra. For these four monolayers, the nuclei were found to have a mean refractive index difference of 1.066 ± 0.007 , a Gaussian distribution of sizes with a mean diameter of $9.9 \pm 0.6 \mu\text{m}$ and a $1/e$ width of the distribution of $0.69 \pm 0.16 \mu\text{m}$. As a check, the photomicrograph of Fig. 2 was directly analyzed to obtain the size distribution of the cell nuclei. Using computer-assisted image analysis, the cell nuclei in the image shown in Fig. 2 were found to have a mean diameter of $10.6 \pm 0.4 \mu\text{m}$, and the distribution of sizes was found to have a width of 0.6 μm , both in good agreement with our a/LCI results.

Subcellular length scale fractal structure

Once the contribution of the cell nuclei to the light-scattering signal has been found, the remaining portion can be analyzed to determine the organization of smaller structures within the nucleus. As described above, the Fourier transform of the a/LCI spectrum gives the two-point correlation function of the electric field scattered by the small struc-

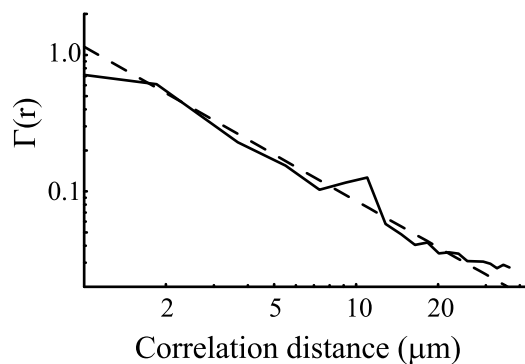


FIGURE 6 Correlation function obtained by Fourier transform of residual light-scattering data. The data (*solid line*) are best fit by a power law (*dashed line*), indicating the self-similar nature of smaller structures within the model epithelial cells.

tures, and thus describes their correlations. Fig. 6 shows the two-point correlation function $\Gamma(r)$, obtained by taking the Fourier transform of the residual distribution of the light-scattering data shown in Fig. 3. Remarkably, the straight line on this log-log plot clearly shows the inverse power law dependence of the correlations, indicating the fractal nature of the light scattering from subcellular structures. In this case we find $\Gamma(r) \propto r^{-\alpha}$, where $\alpha = 1.15$. The exponent of the power law of the correlation function gives insight into the fractal nature of the smaller structures. It is related to the fractal dimension of these structures using Eq. 9, yielding $D = 1.85$. For the 12 spatial points which are examined, the average correlation exponent, $\alpha = 1.21 \pm 0.10$, corresponding to a fractal dimension, $D = 1.79 \pm 0.10$.

Long-range correlations

Information about the organization of the monolayer can also be obtained by analyzing the correlations in the a/LCI spectra (Fig. 4). In this case, subtracting the background from the overall correlation function enables us to visualize the correlations within the monolayer, as shown in Fig. 7. In this plot we see a peak near $10 \mu\text{m}$, corresponding to the size of the cell nuclei and a peak near $16 \mu\text{m}$, possibly corresponding to the size of the cell. The interesting features here are the peaks which appear at correlation lengths of $25\text{--}30 \mu\text{m}$. The peak near $26 \mu\text{m}$ corresponds nicely to the cell nucleus size plus the size of the cell, as one would expect two adjacent nuclei to be separated by approximately one cell diameter. The peak near $32 \mu\text{m}$ similarly corresponds to twice the cell diameter. These correlations contain information about the organization of the cell monolayer and represent the correlated positions of one cell and its nearest neighbor. However, further study with a variety of cell samples will be required for a complete interpretation of this component of the a/LCI spectra.

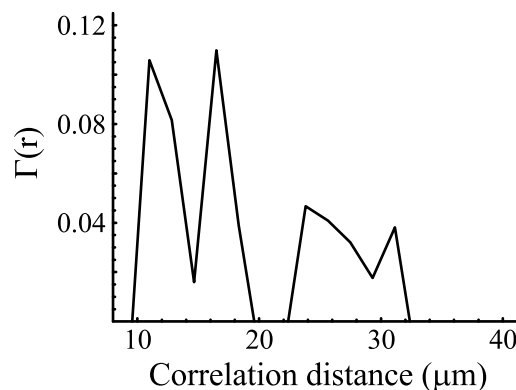


FIGURE 7 Residual correlation function, indicating long-range correlations within the model epithelial cell monolayer. The correlations extend well beyond the size of the cell.

DISCUSSION

The goal of this study was to establish the capability of a/LCI for measuring the subcellular structure of intact, living cells. Using this technique we have measured three aspects of cellular organization and substructure: 1) size distribution of cell nuclei; 2) fractal organization of subcellular structures; and 3) long-range correlations within the monolayer. This section discusses the importance and utility of probing each of these characteristics.

Size distribution of cell nuclei

As described above, LSS techniques have been applied to measuring the size distribution of cell nuclei *in vivo*. In clinical applications, LSS has been used to diagnose precancerous changes associated with neoplasia, in particular, the enlargement and crowding of cell nuclei (Backman et al., 2000). The a/LCI technique also provides a means for probing this morphological feature. However, it provides new capabilities afforded by its interferometry-based approach.

The a/LCI technique shares a common geometry with optical coherence tomography (OCT), a biomedical imaging technique also based on a Michelson interferometer. OCT has been used to obtain *in vivo* microscopic images of subsurface histological tissue structures in a number of clinical applications (Izatt et al., 1997), but it lacks the resolution to quantitatively measure subcellular features. The common optical design permits a/LCI to be used in combination with OCT, which would allow co-registration of histological features with measurements of subcellular structure. The same depth resolution obtained by OCT, which permits imaging of subsurface layers, is achieved in a/LCI. This feature allows measurement of subcellular features at different depths beneath the tissue surface, permitting a detailed assessment of the extent of neoplastic transformation.

Fractal organization of subcellular structure

Another potentially useful ability of a/LCI is its capability to determine the organization of subcellular structures non-destructively, in vivo, and without fixation or staining agents. Interestingly, we have found that there is a fractal behavior in the organization of subcellular structures. Currently, most studies that relate fractal behavior to the development of cancer rely on examining micrographs of cellular structure and then calculating a fractal dimension (Schmitt and Kumar, 1996; Einstein et al., 1998; Pogue et al., 2000). Because these studies examine samples which have been fixed and/or stained, they are subject to the artifacts of preparation and thus suffer from the same impediments which limit histopathology. a/LCI measures correlations through light scattering free of the artifacts of fixation and staining. Thus, it enables more direct connections to be made between cellular structures and their fractal nature, through the power law exponent of the correlation function and the corresponding fractal dimension.

When defined in relation to a mass fractal, as in Eq. 7, the fractal dimension describes the way in which subcellular structures fill space. From the light-scattering data, we are able to extract the fractal dimension ($D = 1.79$) of the subcellular structures of the epithelial cells. This gives a quantitative measure of how the space inside the cell is filled. It will be interesting to study the fractal dimension of cells at different stages of neoplastic transformation and the extent to which changes of the structure of the cell and nucleus are related to changes in their function.

Long-range correlations

The a/LCI technique recovers information about correlations from cell to cell within the monolayer. This information describes the overall order of the cell sample. In the case of the monolayer, the cells have a regular order. However, in biological tissues, the locations of the cells may be less ordered. We believe that a/LCI analysis can also be applied to whole tissues, as well as cell monolayers. It is well known that the degree of organization of an epithelial tissue structure, such as in colon crypts, is an important indicator used by pathologists in clinical diagnosis of disease. The long-range correlations measured by a/LCI provide a quantitative measure of such organization and may be useful in parameterizing neoplastic change. Further studies based on the a/LCI technique will illuminate the relationship between the organization of cells within biological tissues and the health of that tissue.

CONCLUSION

We have demonstrated that structural and organizational information can be recovered from living, intact monolayers

of model epithelial cells using a/LCI. The size distribution of the cell nuclei is measured noninvasively with subwavelength precision. In addition, we are able to measure correlations within the cells, which indicate the self-similar nature of the subcellular structures, as well as correlations between cells, indicating their organization within the monolayer.

This work was conducted at the MIT Laser Biomedical Research Center and was supported by grants from the Hamamatsu Corporation, the National Science Foundation (CHE-0111370) and the National Institute of Health through the National Center for Research Resources (P41-RR02594). Adam Wax is supported by an NRSA fellowship grant from the National Institutes of Health (F32 RR05075-02).

REFERENCES

- Backman, V., R. Gurjar, K. Badizadegan, I. Itzkan, R. R. Dasari, L. T. Perelman, and M. S. Feld. 1999. Polarized light scattering spectroscopy for quantitative measurement of epithelial cellular structures in situ. *IEEE J. Sel. Top. Quantum Electron.* 5:1019–1026.
- Backman, V., M. B. Wallace, L. T. Perelman, J. T. Arendt, R. Gurjar, M. G. Muller, Q. Zhang, G. Zonios, E. Kline, T. McGillican, S. Shapshay, T. Valdez, K. Badizadegan, J. M. Crawford, M. Fitzmaurice, S. Kabani, H. S. Levin, M. Seiler, R. R. Dasari, I. Itzkan, J. Van Dam, and M. S. Feld. 2000. Detection of preinvasive cancer cells. *Nature.* 406: 35–36.
- Backman, V., V. Gopal, M. Kalashnikov, K. Badizadegan, R. Gurjar, A. Wax, I. Georgakoudi, M. Mueller, C. W. Boone, R. R. Dasari, and M. S. Feld. 2001. Measuring cellular structure at submicron scale with light scattering spectroscopy. *IEEE J. Sel. Top. Quantum Electron.* 7:887–893.
- Drezek, R., A. Dunn, and R. Richards-Kortum. 1999. Light scattering from cells: finite-difference time-domain simulations and goniometric measurements. *Appl. Optics.* 38:3651–3661.
- Einstein, A. J., H. S. Wu, and J. Gil. 1998. Self-affinity and lacunarity of chromatin texture in benign and malignant breast epithelial cell nuclei. *Phys. Rev. Lett.* 80:397–400.
- Givan, A. L. 2001. Principles of flow cytometry: an overview. *Methods Cell Biol.* 63:19–50.
- Izatt, J. A., M. D. Kulkarni, K. Kobayashi, J. K. Barton, and A. J. Welch. 1997. Optical coherence tomography for biomedicine. *Opt. Phot. News.* 8:41–47, 65.
- Landau, L. D., and E. M. Lifshitz. 1960. *Electrodynamics of Continuous Media.* Reading, MA, Addison-Wesley. 377.
- Mandel, L., and E. Wolf. 1995. *Optical Coherence and Quantum Optics.* New York, Cambridge University Press. 233.
- Perelman, L. T., V. Backman, M. Wallace, G. Zonios, R. Manoharan, A. Nusrat, S. Shields, M. Seiler, C. Lima, T. Hamano, I. Itzkan, J. Van Dam, J. M. Crawford, and M. S. Feld. 1998. Observation of periodic fine structure in reflectance from biological tissue: a new technique for measuring nuclear size distribution. *Phys. Rev. Lett.* 80:627–630.
- Pogue, B., M. A. Mycek, and D. Harper. 2000. Image analysis for discrimination of cervical neoplasia. *J. Biomed Opt.* 5:72–82.
- Schmitt, J. M., and G. Kumar. 1996. Turbulent nature of refractive-index variations in biological tissue. *Opt. Lett.* 21:1310–1312.
- Teixera, J. 1986. Experimental methods for studying fractal aggregates. *In* On Growth and Form, Fractal and Non-Fractal Patterns in Physics. H. E. Stanley and N. Ostrowsky, editors. Nijhoff, Boston, MA. 145–162.
- Tuchin, V. V. 2000. *Tissue Optics: Light Scattering Methods and Instruments for Medical Diagnosis.* SPIE, Bellingham, WA.
- van de Hulst, H. C. 1957. *Light Scattering by Small Particles.* Dover Publications, New York.

- Wax, A., and J. E. Thomas. 1996. Optical heterodyne imaging and Wigner phase space distributions. *Opt. Lett.* 21:1427–1429.
- Wax, A., C. Yang, V. Backman, M. Kalashnikov, R. R. Dasari, and M. S. Feld. 2001a. Determination of particle size using the angular distribution of back-scattered light as measured with low-coherence interferometry. *J. Opt. Soc. Am. A. Opt. Image Sci. Vis.* 19:737–744.
- Wax, A., C. Yang, R. R. Dasari, and M. S. Feld. 2001b. Angular light scattering studies using low-coherence interferometry. In *Coherence Domain Optical Methods in Biomedical Science and Clinical Applications*. V. V. Tuchin, J. A. Izatt, and J. G. Fujimoto, editors. *Proc. SPIE*. 4251:32–42.
- Wax, A., C. H. Yang, R. R. Dasari, and M. S. Feld. 2001c. Measurement of angular distributions by use of low-coherence interferometry for light-scattering spectroscopy. *Opt. Lett.* 26:322–324.
- Yang, C. H., L. T. Perelman, A. Wax, R. R. Dasari, and M. S. Feld. 2000. Feasibility of field-based light scattering spectroscopy. *J. Biomed. Opt.* 5:138–143.